Title
Fly eyes are not still: a motion illusion in Drosophila flight supports parallel visual processing

Journal
Journal of Experimental Biology, 223(10)

ISSN
0022-0949

Authors
Salem, Wael
Cellini, Benjamin
Frye, Mark A
et al.

Publication Date
2020-05-15

DOI
10.1242/jeb.212316

Peer reviewed

Fly eyes are not still: a motion illusion in *Drosophila* flight supports parallel visual processing

Wael Salem[1], Benjamin Cellini[1], Mark A. Frye[2], Jean-Michel Mongeau[1*]

[1] Department of Mechanical Engineering, Pennsylvania State University, University Park, PA 16802

[2] Department of Integrative Biology and Physiology, University of California - Los Angeles, Los Angeles, CA 90095-7239

*Corresponding author:

Jean-Michel Mongeau

204 Reber Bldg

Pennsylvania State University

University Park, PA 16802

jmmongeau@psu.edu

ABSTRACT

Most animals shift gaze by a ‘fixate and saccade’ strategy, where the fixation phase stabilizes background motion. A logical prerequisite for robust detection and tracking of moving foreground objects, therefore, is to suppress the perception of background motion. In a virtual reality magnetic tether system enabling free yaw movement, *Drosophila* implemented a fixate and saccade strategy in the presence of a static panorama. When the spatial wavelength of a vertical grating was below the Nyquist wavelength of the compound eyes, flies drifted continuously and gaze could not be maintained at a single location. Because the drift occurs from a motionless stimulus—thus any perceived motion stimuli are generated by the fly itself—it is illusory, driven by perceptual aliasing. Notably, the drift speed was significantly faster than under a uniform panorama suggesting perceptual enhancement due to aliasing. Under the same visual conditions in a rigid tether paradigm, wing steering responses to the unresolvable static panorama were not distinguishable from a resolvable static pattern, suggesting visual aliasing is induced by ego motion. We hypothesized that obstructing the control of gaze fixation also disrupts detection and tracking of objects. Using the illusory motion stimulus, we show that magnetically tethered *Drosophila* track objects robustly in flight even when gaze is not fixated as flies continuously drift. Taken together, our study provides further support for parallel visual motion processing and reveals the critical influence of body motion on visuomotor processing. Motion illusions can reveal important shared principles of information processing across taxa.

KEYWORDS: motion vision, feedback, control, saccade, stability

INTRODUCTION

Animals must be able to identify and classify objects rapidly to generate appropriate behavior. For example, a fly must identify and classify potential predators while moving through a background of foliage. Complicating this process is that locomotion itself generates a moving retinal background image. Subject to ego motion, animals should be able to detect foreground objects more easily if the retinal image of the background is stabilized. Complicating gaze stabilization, however, is that the eyes are never truly still: for instance, in *Calliphora*, the head is in constant motion in free flight (Hateren and Schilstra, 1999) and our own eyes constantly move due to microsaccades, drift and tremor (Martinez-Conde and Macknik, 2017). At present, it is not well understood whether an animal can detect and track object motion better when still than in motion (Land and Nilsson, 2012).

Seminal work in *Musca* showed that a fly can readily discriminate an object from the background (Egelhaaf, 1985; Reichardt and Poggio, 1979). Recent work in *Drosophila* revealed that object tracking is spatially distinct from background stabilization, implying that the two systems are distinct (Fox et al., 2014). More recent work in magnetically tethered flies free to pivot showed that detection and tracking of a visual object is enabled by rapid switching between the smooth optomotor reflex that stabilizes the background and saccades that track a foreground object (Keleş et al., 2019; Mongeau and Frye, 2017; Mongeau et al., 2019), further supporting that gaze stabilization and object tracking are implemented by distinct controllers. Flies rely on a velocity-based controller that reduces retinal slip while simultaneously integrating object position spatiotemporally (Mongeau and Frye, 2017), therefore it would appear that these two systems are not only distinct but also operate in parallel. With this contention, we would hypothesize that disruption of one controller, say the velocity controller that stabilizes

58 background motion, would not interfere with the position- or Figure-motion (FM)-based
59 controller for object tracking (Aptekar et al., 2012). Walking flies that are motion blind by
60 blocking T4/T5 pathways can track an object, suggesting parallel control systems (Bahl et al.,
61 2013). However, other work suggests that object-ground discrimination in flight does not require
62 parallel processing, but can instead rely on asymmetric processing by Horizontal-System (HS)-
63 like cells (Fenk et al., 2014). Therefore, at present, there are two distinct hypotheses : 1) object
64 and ground discrimination is processed by parallel pathways and 2) object and ground
65 discrimination is asymmetrically processed by overlapping pathways.

66 To distinguish between these two hypotheses, we used a magnetic pivot enabling free
67 rotation in yaw (Figure 1A,B). We developed a paradigm that visually hindered the gaze
68 stabilization reflex by presenting flies a grating below the supposed maximum resolvable spatial
69 wavelength of the *Drosophila* visual system (spatial wavelength λ = 7.5° and 3.75°). For the
70 multifaceted, hexagonal lattice eyes of *Drosophila*, $1/(\sqrt{3}\Delta\varphi)$ is the smallest spatial frequency
71 of a vertical grating that the eye can resolve where $\Delta\varphi$ is the angle between adjacent ommatidia
72 (Figure 1C) (Snyder, 1979). When λ of a stimulus is less than $\sqrt{3}\Delta\varphi$, the retinal image is under
73 sampled, resulting in perceptual aliasing. *Drosophila* have an approximate inter-ommatidial
74 angle range of 4.5–6° (mean = 4.5°) along the horizontal (yaw) axis (Gonzalez-Bellido et al.,
75 2011), and thus theoretically the Nyquist wavelength of *Drosophila* is ~9°, although the actual
76 cutoff also depends on facet and rhabdomere diameter as well as retinal noise levels and
77 background luminance. Indeed, dark adapted eyes experience an increase in acceptance angle
78 and resolving the edges of a high-frequency pattern requires more photons (Gonzalez-Bellido et
79 al., 2011; O'Carroll and Wiederman, 2014). Acuity at high spatial frequencies is further
80 attenuated by diffraction phenomena and rhabdomere geometry, that together define the

acceptance angle $\Delta\rho$ (Buchner, 1984). The acceptance angle further limits the effective cut-off frequency of the optical system as $1/\Delta\rho$, which for *Drosophila* is approximately 1/5° (Gonzalez-Bellido et al., 2011). For receptors that are diffraction limited, the contrast ratio decreases to nearly zero at the cutoff frequency (Figure 1D) (Buchner, 1984; Land, 1997), where the contrast ratio is defined as

$$M(v) = e^{-3.56(v\Delta\rho^2)} \quad (1)$$

where v is the spatial frequency and $\Delta\rho$ is the acceptance angle which is approximately 5° for *Drosophila* (Buchner, 1984). Animal eyes therefore trade-off acuity and contrast sensitivity as decreasing $\Delta\varphi$ increases acuity but concomitantly decreases contrast sensitivity, as contrast sensitivity is itself proportional to the ommatidial diameter (Land and Nilsson, 2012).

Behavioral experiments in tethered, walking and flying *Drosophila* showed that the turning response to a rotating grating decreases near zero at the Nyquist wavelength and curiously reverses below Nyquist wavelength, indicating perceptual aliasing (Buchner, 1976; Gotz, 1965). The same effect was demonstrated in bees (Kunze, 1961). However, at present it is not known how the behavioral results by Buchner and Gotz in tethered preparations manifest in more naturalistic closed-loop conditions. Furthermore, a recent study challenges the notion that *Drosophila* ocular spatial resolution is limited by the interommatidial distance by showing that rapid rhabdomere contraction can generate hyperacute vision below aliasing wavelength, enabling discrimination of a grating with spatial wavelength as low as 1.16° (Juusola et al., 2017). Low background luminance levels in Buchner's work (16 cd m^{-2}) would have generated very low R1-R6 photoreceptor outputs, rendering it difficult to resolve hyperacute visual patterns (Juusola et al., 2017). It is at present unclear whether hyperacuity is observable under more

naturalistic flight conditions where animals experience ego motion and hence sensory reafference. Specifically, can flies stabilize a grating below the aliasing limit in closed loop?

Here, we show that when presented a static grating at or near Nyquist wavelength in a magnetic tether, flies could not maintain gaze at a single location: instead, flies drifted continuously. Under the same visual conditions in a rigid tether system, flight responses were not distinguishable from responses to a resolvable pattern, suggesting that in the magnetic tether self-motion induces a motion illusion driven by perceptual aliasing. We then tested whether flies could detect and track an object at all when gaze is not fixated due to perceptual aliasing of the background. We presented flies a high contrast, moving object superimposed over a $\lambda = 7.5°$ static grating. We show that gaze fixation is not necessary for closed-loop object pursuit, thereby providing further support for the hypothesis that background stabilization and object tracking controllers operate in parallel (Figure 1E).

METHODS

Animals

A wild-type *Drosophila melanogaster* strain was maintained at 25°C under a 12 h:12 h light:dark cycle with access to food and water *ad libitum*. This *Drosophila melanogaster* strain was reared from a wild caught iso-female line. All experiments were performed with 3- to 5-day-old adult female flies.

Magnetic tether paradigm

Animals were prepared for each experiment according to a protocol that has been described previously (Bender and Dickinson, 2006a; Duistermars and Frye, 2008). Flies were cold-anesthetized by cooling on a stage maintained at approximately 4°C. For the magnetic tether, stainless steel pins (100 µm diameter; Fine Science Tools, Foster City, CA) were glued onto the thorax by applying UV-activated glue. Flies were allowed at least one hour to recover before running experiments.

The magnetic tether system has been described elsewhere (Bender and Dickinson, 2006a; Duistermars and Frye, 2008). The display consisted of an array of green (570 nm) 96 × 16 light emitting diodes (LEDs) that wrap around the fly, subtending 360° horizontally and 56° vertically (Figure 1A), therefore each pixel on the visual horizon subtended 3.75° on the eye. Panel LED matrices operated at a wavelength of 570 nm. Flies were suspended between two magnets, allowing free rotation along the vertical (yaw) axis and illuminated from below with an array of eight 940 nm LEDs (not shown). The angular position of the fly within the arena was recorded at 160 frames s^{-1} with an infrared-sensitive camera placed directly below the fly (A602f, Basler, Ahrendburg, Germany). The LED arena operated at maximum intensity with a mean luminance

of approximately 72 cd m^{-2}. We also used a larger LED display system with 192 × 40 LEDs—twice the diameter of the 96 × 16 display—with each pixel subtending 1.875° on the eye.

After suspending flies within the magnetic field, flies were given several minutes to acclimate. We began each experiment by eliciting sustained rotation of the fly by revolving a visual panorama either clockwise or counterclockwise for 30 s at 120° s^{-1}. This stimulus elicited a strong rotatory, smooth co-directional optomotor turning response with occasional saccades. From these data, we estimated the fly's center of rotation by computing the cumulative sum of all camera frames and measuring its centroid. Any fly that could not robustly follow the rotating panorama was not used for experiments. We presented each stimulus for a period of 20−30 s, defining the duration of an individual trial. Between trials, we presented a fixed visual landscape for 25 s for the fly to rest. The procedure to identify saccades from heading data has been described elsewhere (Mongeau and Frye, 2017). We modeled the fly as an ellipsoid and determined the heading by calculating the major axis of the ellipse in each video frame. The asymmetry between head and abdomen along the longitudinal axis was used to determine the direction of the fly heading vector.

Rigid tether paradigm

After cold-anesthetizing flies at 4°C, we affixed a small tungsten pin onto the thorax using UV-activated glue. Flies recovered for at least one hour prior to experiments. Flies were then placed in the center of a cylindrical flight arena with the same pixel size and color wavelength as the magnetic tether paradigm (Figure 4A). The arena has been described elsewhere (Reiser and Dickinson, 2008). The display consisted of a cylindrical array of 96 × 32 LEDs subtending 330° horizontally and 94° vertically. An infrared diode (940 nm) projected light onto the wings, casting a shadow unto two separate optical sensors. A custom wingbeat

analyzer (JFI Electronics, Chicago, IL, USA) transformed the signal from each optical sensor into a signal proportional to the wingbeat amplitude (defined as left minus right wing). Changes in wingbeat amplitude (ΔWBA) signals from the optical wingbeat analyzer were acquired at 1000 Hz. The LED arena operated at maximum intensity with a mean luminance of approximately 72 cd m^{-2}.

Paper grating

To determine the possible effect of the LED arena on the behavioral response in the magnetic tether, we printed a black-and-white grating on white paper using a laser printer with a resolution of 4800 × 1200 dots per inch. The paper grating had the same overall diameter and height as the magnetic tether LED arena with $\lambda = 7.5°$. Using full room white illumination with flicker frequency above the *Drosophila* visual system (Cosens and Spatz, 1978), we measured the mean luminance inside the paper drum to be ~80 cd m^{-2} (Tondaj LX-1330B), which was similar to the LED arena luminance (72 cd m^{-2}). For the trials with a paper pattern and the larger LED arena, we used the fly's observed drift to compute the center of rotation.

Elementary Motion Detector (EMD) Model

Computational model

We implemented an EMD model as previously described for *Drosophila* visual physiology (Dickson et al., 2008; Tuthill et al., 2011). We modeled a single array of 1×72 ommatidia. We modeled the optical, spatial low-pass filter for each ommatidium using a Gaussian function of the form

$$G(\zeta) = e^{\frac{-4\ln(2)\zeta^2}{\Delta\rho^2}} \quad (2)$$

where ζ is the angle from the optical axis of the ommatidium and $\Delta\rho$ is the acceptance angle. Here we used $\Delta\rho = k\Delta\phi$ where $\Delta\phi$ is the inter-ommatidial angle (fixed at 4.5°) and k = 1.1, as previously measured (Buchner, 1984). We computed the image by convolving an intensity signal $I(\zeta,k)$, where k is the discrete sample time, with the acceptance angle of the modeled ommatidia

$$V(k) = G(\zeta) * I(\zeta, k) \tag{3}$$

We used the Hassenstein-Reichardt, delay-and-correlate EMD model such that the output $V_{EMD}(k)$ of adjacent photoreceptors A and B is defined as

$$V_{EMD}(k) = V'_A(k)V_B(k) - V_A(k)V'_B(k) \tag{4}$$

where $V_A(k)$ and $V_B(k)$ are the output of the two photoreceptors and $V'_A(k)$ and $V'_B(k)$ are the delayed outputs of the same photoreceptors by a first-order delay filter of the form

$$f(t) = \frac{1}{\tau} e^{\frac{-k}{\tau}} \tag{5}$$

where τ is the time constant (set at 40 ms). We computed the EMD response by summing across all simulated ommatidia and taking the mean of the sum at each temporal frequency.

Analytical model

We also simulated an analytical model of the EMD subject to a sinusoidal input signal (Borst et al., 2003). The steady-state response $\langle R \rangle$ of the i th detector located at φ

$$\langle R_i \rangle_\varphi = \Delta I^2 \cdot \sin\left(2\pi \frac{\Delta\varphi}{\lambda}\right) \frac{\tau\omega}{1 + (\tau\omega)^2} \tag{6}$$

where ΔI is the contrast of the pattern, τ is the time constant of the low-pass, first-order temporal filter, $\Delta\varphi$ is the inter-ommatidial angle (spacing of detector), ω is the angular frequency of the

stimulus and λ is the spatial wavelength of the pattern. Here we used ΔI = 1 (full contrast), τ = 40 ms, and $\Delta\varphi$ = 4.5°. This model assumes a sinusoidal grating of the form

$$x(t) = \bar{I} + \Delta I \cdot \sin\left(2\pi \frac{v}{\lambda} t + \varphi\right) \quad (7)$$

where v is the constant angular velocity of the stimulus and $\bar{I}$ is the mean luminance. This model, unlike the computational model described above, does not take into consideration the filtering optics of the compound eye defined by acceptance angle.

Spatio-Temporal Action Field (STAF)

To quantify the bar tracking effort of flies in the rigid tether paradigm, we used a previously described STAF technique (Aptekar et al., 2014). We determined the impulse response function of a fly at 24 uniformly spaced azimuthal locations by convolving the fly's steering response (ΔWBA) with a pseudo-random, maximum length shift register sequence (m-sequence) prescribing bar position for each trial (MacWilliams and Sloane, 1976) (Figure 5D–F). The m-sequence prescribed positive (+1) and negative (-1) steps controlling bar position, with each step corresponding to one pixel or 3.75° angular displacement of the bar (Figure 5D). For each fly, the position of the bar was randomized at the prescribed 24 locations. For each test period, we presented three periods of a 127 element (7^{th} order) m-sequence. The visual scene was updated at a frame rate of 25 Hz or every 40 ms such that each update was perceptually instantaneous. The refresh rate of the LED arena was approximately 2.6 MHz (Reiser and Dickinson, 2008). Each trial lasted 15.6 s with a total experimental time for each fly of ~28 minutes. To keep the fly motivated after each trial, we presented a bar under virtual closed-loop for 5 s.

Statistical analysis

All statistical analysis was performed using Matlab (Mathworks, Natick, MA, USA) and JMP (SAS, Cary, NC, USA). Unless otherwise specified, we report mean ± 1 standard deviation. When displaying box plots, the central line is the median, the bottom and top edges of the box are the 25th and 75th percentiles and the whiskers extend to ± 2.7 standard deviations.

Data Availability

All data and custom-written software are available by contacting the corresponding author.

RESULTS

We presented static, wide-field panoramas of different spatial wavelengths to flies that were free to rotate in yaw in a magnetic pivot (Figure 1A). As expected, under these visual conditions, flies generated occasional saccades interspersed by periods of gaze stabilization between saccades (Figure 2A). We challenged the operation of the gaze stabilization reflex by presenting flies with a grating of light and dark stripes at a spatial wavelength λ of 7.5°, near the maximum resolvable spatial wavelength of the *Drosophila* visual system. At λ = 7.5° the perceived contrast ratio for *Drosophila* is ~1% due to the ommatidial acceptance angle, leaving little-to-no detectable features in the panorama, thus we hypothesized that the panorama should be ambiguous (Figure 1D). Curiously, at λ = 7.5° flies smoothly drifted whereas flies maintained stable headings when presented gratings of higher spatial wavelengths (Figure 2A). To illustrate this peculiar result further, we simulated two-dimensional flight trajectories from angular heading data by prescribing a constant flight speed (30 cm s^{-1}). This simulation illustrates the tortuous fight trajectory at λ = 7.5° compared to other spatial wavelengths (Figure 2B). To quantify the amount of drift, we 1) separated the data set into flies that on average turned more clockwise (CW) or counter-clockwise (CCW) against the stationary background grating and 2) removed saccades from the smooth angular heading data using custom algorithms. Across all animals and trials, these data confirmed that the drift is strongly present at λ = 7.5° but not at other wavelengths (Figure 2C−E). Animals did not preferentially drift CW or CCW (χ^2 test, DF = 1, p = 0.666). In some trials at λ = 7.5° (16% of all trials), flies spontaneously changed direction.

The peculiar result that *Drosophila* drifts in the presence of a static panorama composed of near-minimum resolvable spatial wavelength demonstrates that the optomotor reflex is

perpetually active in closed-loop to stabilize gaze by reducing retinal slip generated by ego-motion. At $\lambda = 7.5°$ flies are generating reafferent optic flow from their own motion (Figure 3A). One possibility is that flies cannot eliminate reafferent optic flow to stabilize gaze because their eyes presumably cannot detect or resolve high-contrast, high-frequency edges. Furthermore, motion of the fly itself due to destabilization of optokinetic reflexes may further exacerbate the detection of high contrast features due to motion blur. Motion blur, a result of temporal integration, manifests first as a loss of contrast to the highest spatial frequencies (Snyder, 1979). Taken together, at $\lambda = 7.5°$ the closed-loop gaze stabilization reflex may become effectively an unstable closed-loop control system in which the reafferent and efferent information are not properly cancelled, i.e. a difference perceived *vs.* actual body velocity, leading to non-zero net body velocity (Figure 3A). We tested whether flies cannot in fact resolve features of sufficient contrast at $\lambda = 7.5°$ by presenting flies a uniformly lit panorama. Indeed, for a contrast ratio of 1% with a pattern of $\lambda = 7.5°$, we might expect flies to respond no differently than in the presence of a uniform panorama. Although flies drifted significantly more in the presence of a uniform panorama than panoramas of $\lambda = 15–90°$, the effect was less pronounced than under $\lambda = 7.5°$ (Figure 2C−E). Flies presented a $\lambda = 7.5°$ pattern drifted at a median speed of $8°s^{-1}$ which was statistically significant from drifting speed in the presence of a uniform background (median $= 2°s^{-1}$; *t*-test, $p<0.001$), suggesting that aliasing effects enhance the motion illusion due to perceptual aliasing (Figure 2E).

To verify that yaw drifting at $\lambda = 7.5°$ was not an artefact of the visual display (LED arena, see Methods), we repeated the same experiment under similar mean luminance levels with a black-and-white striped drum printed on white paper. Although flies drifted less on average with a paper drum than the LED arena, the effect was nonetheless considerable, with a median

rotation speed of 2°s^{-1}, resembling the effect of the uniform grating (Figure 2F). Notably, the paper grating was under broadband white light illumination whereas the LED panels operated within a wavelength range centered at 570 nm, slightly above the optimal wavelength for the maximum optomotor response (Heisenberg and Buchner, 1977). The drift speed at λ = 7.5° on paper was significantly larger than for λ > 7.5° in the LED arena (*t*-test with λ > 7.5° wavelengths pooled, p<0.001). As another control, we tested flies in a virtual reality arena with twice the diameter, and therefore twice the spatial resolution (subtending 1.875° per pixel) but the same mean background luminance. When presented a λ = 7.5° static grating (2 pixels ON, 2 pixels OFF repeating), flies generated significant drift (median = 5°s^{-1}), comparable to the arena with lower resolution (Figure 2G). The same flies presented a λ = 3.75° grating also drifted considerably, although less so than at 7.5° (median = 2°s^{-1}; *t*-test, p<0.001, n = 5 flies, 25 trials)(Figure 2G). The difference between 7.5° and 3.75° suggests that aliasing near Nyquist wavelength generates larger drift and therefore enhances the motion illusion effect, whereas λ much smaller than the Nyquist wavelength limit appears more like a spatially uniform background. Taken together, these results suggest that drift experienced by flies was robust and largest at λ = 7.5°, with some effects due to the type of background (LED vs. paper) and pixel resolution (1.875° vs. 3.75°).

The λ = 7.5° pattern is near the predicted Nyquist wavelength, but for *Drosophila* it is closer to 9° based on the average inter-ommatidial distance along the yaw axis (Gonzalez-Bellido et al., 2011). To test whether there is a difference in fly response between a 7.5 and 9° spatial wavelength pattern, we presented flies a static paper pattern at these two spatial wavelengths. Overall, the drift speed was similar under both conditions (Kruskal-Wallis, p =

0.102; 7.5°: n = 17 flies; 9°: n = 12 flies), suggesting similar visual aliasing influences at λ = 7.5° and 9° (Figure 2F).

Interestingly, flies on average generated the same number of spontaneous saccades across all spatial wavelengths (Pearson test, p = 0.781, 6,546 saccades; median saccade frequency = $0.36°s^{-1}$), suggesting that saccades were generated even when gaze is not maintained at a single location, supporting the notion that some saccades are triggered by spontaneous processes. Overall the spontaneous saccade rate was consistent with previous studies (Bender and Dickinson, 2006a; Ferris et al., 2018; Mongeau and Frye, 2017) and there was no robust influence of spatial properties of the panorama on saccade dynamics (Figure 2H).

To test whether the λ = 7.5° pattern is resolvable, we simulated the computational response of a Hassenstein-Reichardt EMD (Figure 3B). As predicted from an EMD analytical model subject to a sinusoidal input, aliasing, i.e. negative EMD outputs, should occur within the spatial frequency range $1/\Delta\varphi > 1/\lambda > 1/2\Delta\varphi$ (Figure 3C). For the analytical model, a pattern of λ = 7.5° generated a comparatively large negative steady-state EMD output when compared to resolvable visual stimuli, corroborating previous results by Buchner and Gotz (Buchner, 1984; Gotz, 1965) (Figure 3D,E). In contrast, the computational model, which includes an optical spatial filter, generated a comparatively small negative EMD output for λ = 7.5°. Therefore the analytical model, without simulating eye optics, can potentially overestimate the biological motion detector response and therefore also the predicted flight behavioral responses. The analytical EMD model predicted a large positive EMD response at λ = 3.75° whereas the computational model predicted little-to-no response. Our experimental results showed that flies drift significantly at λ = 3.75°, therefore these results do not agree with the EMD model predictions. Taken together, the EMD output can predict visual aliasing near the Nyquist spatial

wavelength of the eye, with different predictions in relative magnitude based on the type of EMD model implemented. Whereas a $\lambda = 7.5°$ pattern is resolvable to *Drosophila*, because the drift occurs from a motionless static stimulus, we conclude that it is illusory and driven by perceptual aliasing (Figure 3A).

If flies cannot maintain a constant gaze at $\lambda = 7.5°$, can they detect and pursue a superimposed moving object? If the gaze stabilization reflex and the object pursuit systems are indeed parallel control systems, then we would expect object pursuit to be intact when the gaze stabilization reflex is obstructed, provided that the object is of sufficient contrast and its motion is not blurred. We previously showed that flies robustly track a moving object superimposed on a counter-rotating ground, enabled by rapid switching between smooth movement gaze stabilization and object detection and saccadic pursuit (Mongeau and Frye, 2017). We repeated this experiment but added one condition in which the object rotated superimposed on a grating of $\lambda = 7.5°$. Under these conditions, we hypothesized that the low contrast background pattern should elicit weak or no responses due to the presence of a highly salient foreground feature. As previously observed (Mongeau and Frye, 2017), when moving an object on a broadband randomly textured ground, flies switched between bouts of saccadic tracking in pursuit of the object and smooth gaze stabilization between saccades (Figure 4A). When the object exited the field of view, flies primarily generated smooth turns at rotational body velocity near unity gain (Mongeau and Frye, 2017). From these results, we would predict that gaze stabilization is important for object fixation since gaze is rapidly stabilized between saccades, within as little as 20 ms from the termination of a saccade (Mongeau and Frye, 2017). Therefore, we predicted that flies cannot stabilize an object on a $\lambda = 7.5°$ grating. Strikingly, when the object moved on the $\lambda = 7.5°$ grating, object pursuit was intact (Figure 4A). Flies generated robust bouts of tracking

saccades even if they could not maintain a constant gaze, as evidenced by periods of drifting heading between saccades (Figure 4A bottom). Flies generated more object tracking saccades on a static λ = 7.5° grating than a rotating background across all background speeds for a balanced experimental design (Figure 4B). At higher background speeds, we suspect that it was more challenging for flies to switch between gaze stabilization and object pursuits as evidenced by the decreasing number of tracking saccades (Figure 4B).

We showed that drift is generated by a static grating near Nyquist frequency, but are these effects manifest in an open-loop paradigm where sensory reafference is less natural? Under the same visual conditions in a rigid tether arena restricting body movement but not head movement, we tested whether Δwing-beat amplitude (ΔWBA) signals might be biased in the presence of a 7.5° background (Figure 5A,B), where ΔWBA provides an indirect measurement of steering torque (Tammero et al., 2004). WBA signals in the presence of a 7.5° grating were not distinguishable from WBA signals in the presence of a resolvable static pattern (paired *t*-test, p=0.900, n = 13 flies), suggesting body-motion-induced visual drift in more natural conditions (magnetic tether) which cannot be captured in an open-loop paradigm (rigid tether)(Figure 5C; Fig. S1). Without fictive drift in an open-loop, rigid-tether paradigm, it would follow that object fixation should remain intact. In particular, is intact object detection and fixation under an illusory background dependent on sensory reafference due to ego-motion? To test this, we used the Spatio-Temporal Action Field (STAF) paradigm with rigidly tethered flies that were free to move their head thereby generating much less ego-motion than in the magno tether (Aptekar et al., 2012; Aptekar et al., 2014). A bar superimposed on a λ = 7.5° static background moved pseudo-randomly, centered at distinct locations in azimuth, from which spatially distinct impulse response functions relating bar motion and wing steering response can be computed (Figure 5D,

E). Measuring impulse responses at 24 distinct locations along the azimuth generate the STAF profile, which, as expected, exhibited a stereotyped spatial tuning for bar steering responses (Figure 5F) similar to those generated for random background patterns in our previous work (Fox et al., 2014). Therefore, in the presence of the $\lambda = 7.5°$ static background, flies robustly tracked the bar.

DISCUSSION

Visual illusions have been demonstrated in a number of vertebrate and invertebrate animals, illustrating common visual processing principles across taxa (Srinivasan, 1993). For instance, flies respond robustly to the reverse-phi motion illusion (Tuthill et al., 2011), contrast illusion (Bahl et al., 2015), and even the waterfall illusion (Srinivasan, 1993). Here, we describe a motion illusion in insects for ambiguous static gratings driven by ego motion, which appears analogous to static motion illusions reported in vertebrates. For instance, static motion illusions have been described in a number of human psychophysics studies, perhaps the most famous being the rotating snake illusion reported by Akiyoshy Kitaoka (Kitaoka A, 2002). Such static motion illusions have been linked to microsaccade production in humans (Otero-Millan et al., 2012; Troncoso et al., 2008). Our results support the notion that just as in humans, as long as the body is mobile fly eyes are never still, and thus ego motion can generate visual illusions not observable in open-loop, rigid tether paradigms even if the head is mobile (Figure 5). Indeed, flies in a magnetic tether are never fully still during inter-saccade intervals, as would be predicted for free flight (Figure 2) (Bender and Dickinson, 2006a). Our results are consistent with visual feedback being critical during periods of straight flight (Bender and Dickinson, 2006b).

In previous work, Buchner observed perceptual aliasing in tethered, walking flies when presented moving gratings with spacing below the Nyquist wavelength (Buchner, 1976). Specifically, in the range $\varphi < \lambda < 2\varphi$, flies turned in the direction opposite to the direction of motion. Buchner also showed that the turning response is attenuated below Nyquist wavelength due to a decrease in contrast ratio. However, recent work (Juusola et al., 2016) challenged Buchner's classic work, showing that perceptual aliasing is absent down to a spatial wavelength

of 1.16°. Juusola et al. argued that the mean stimulus light intensity was low in Buchner's work (16 cd m^{-2}), causing R1-R6 photoreceptors to be unable to resolve fine patterns. Our LED arena pattern has approximately five times the mean luminance reported in Buchner's work, thereby rendering it difficult to predict results in our magno tether in light of work by Buchner. Notably, Buchner's work predicts that flies would respond no differently to a stationary grating near Nyquist than to a uniform panorama., but we found that this is not the case (Figure 2). Thus, a main novelty with regards to the presentation of high frequency gratings in the magno tether is that a static stimulus causes significant and robust illusory motion.

Here we show that a motion illusion supports the hypothesis that object detection and tracking operate in parallel with ground stabilization, suggesting two distinct control systems (Figure 1E). Our results corroborate open-loop flight studies that showed that flies can track an object in virtual reality closed-loop superimposed on a background with opposite gain (Fox et al., 2014)—thereby lending support to the parallel control system hypothesis—but it remained unclear whether these results extended to more natural flight where flies move their body and therefore generate ego motion. Notably, in the magnetic tether apparatus, behavior operates under closed-loop feedback conditions—rather than simulated closed-loop feedback conditions in rigidly tethered flight—so flies experience naturalistic mechanosensory and visual reafference signals and prescribe their own optomotor gains. Indeed, studying flight in closed-loop made possible our discovery that a pattern of λ = 7.5° disrupts gaze fixation, i.e. the same experiment in open-loop generates no fictive drift (Figure 5). This finding extends our previous results which showed that flies can robustly track an object on a counter-rotating background, because under these conditions flies operated near a gain of 1 and therefore experienced little retinal slip (Mongeau and Frye, 2017), whereas under the motion illusion flies could not stabilize retinal slip

and instead drifted continuously (Figure 2A, 4A). This study adds to a growing body of evidence that parallel visual processing enables robust object detection and pursuit in insect flight (Aptekar et al., 2012; Bahl et al., 2013; Fox et al., 2014).

A recent study showed that microsaccadic sampling via rhabdomere contraction can provide *Drosophila* hyperacuity, whereby tethered flies generate an open-loop optomotor response with a grating as small as 1.16° in spatial wavelength, well below aliasing limits (Juusola et al., 2017). Pixels in our LED arena subtend a maximum angle of 3.75° onto the fly's retina (and 1.875° in the larger arena), previously thought to be below acuity as determined by the inter-ommatidial distance (Gonzalez-Bellido et al., 2011; Reiser and Dickinson, 2008). Even with a paper grating and higher resolution display, flies drifted considerably (Figure 2F,G), demonstrating that the motion illusion is robust rather than an artefact of the LED arena. For hyperacuity to manifest in the magnetic tether, we would have expected flies to stabilize gaze for gratings below the aliasing limit, but instead flies drifted continuously. We speculate that the drift is driven by visual processes and that mechanosensory information from halteres likely cannot sense the drift as the angular body velocity is well below haltere sensitivity about the yaw axis (Sherman and Dickinson, 2003). Taken together, we show that hyperacuity is not manifest under more natural closed-loop conditions where the body can pivot about yaw and thus continuously generate small ego motion.

ACKNOWLEDGEMENTS: We thank undergraduates Allie Solomon and Farhaad Khan for laboratory assistance.

AUTHOR CONTRIBUTIONS: Conceptualization: J.M.M., M.A.F.; Data collection: W.S., J.M.M.; Data analysis: W.S., B.C., J.M.M.; Writing: J.M.M., M.A.F.

FUNDING: This work was funded by the National Institutes of Health R01EY026031 (MAF).

REFERENCES

Aptekar, J. W., Shoemaker, P. A. and Frye, M. A. (2012). Figure tracking by flies is supported by parallel visual streams. *Curr. Biol.* **22**, 482–487.

Aptekar, J. W., Keles, M. F., Mongeau, J.-M., Lu, P. M., Frye, M. A. and Shoemaker, P. A. (2014). Method and software for using m-sequences to characterize parallel components of higher-order visual tracking behavior in Drosophila. *Front. Neural Circuits* **8**, 130.

Bahl, A., Ammer, G., Schilling, T. and Borst, A. (2013). Object tracking in motion-blind flies. *Nat. Neurosci.* **16**, 730–8.

Bahl, A., Serbe, E., Meier, M., Ammer, G. and Borst, A. (2015). Neural Mechanisms for Drosophila Contrast Vision. *Neuron* **88**, 1240–1252.

Bender, J. A. and Dickinson, M. H. (2006a). Visual stimulation of saccades in magnetically tethered Drosophila. *J. Exp. Biol.* **209**, 3170–82.

Bender, J. A. and Dickinson, M. H. (2006b). A comparison of visual and haltere-mediated feedback in the control of body saccades in Drosophila melanogaster. *J. Exp. Biol.* **209**, 4597–606.

Borst, A., Reisenman, C. and Haag, J. (2003). Adaptation of response transients in fly motion vision. II: Model studies. *Vision Res.* **43**, 1311–1324.

Buchner, E. (1976). Elementary movement detectors in an insect visual system. *Biol. Cybern.* **24**, 85–101.

Buchner, E. (1984). Behavioural Analysis of Spatial Vision in Insects. In *Photoreception and*

Vision in Invertebrates, pp. 561–621. Boston, MA: Springer US.

Cosens, D. and Spatz, H. C. (1978). Flicker fusion studies in the lamina and receptor region of the Drosophila eye. *J. Insect Physiol.* **24**, 587–594.

Dickson, W. B., Straw, A. D. and Dickinson, M. H. (2008). Integrative Model of Drosophila Flight. *AIAA J.* **46**, 2150–2164.

Duistermars, B. J. and Frye, M. (2008). A Magnetic Tether System to Investigate Visual and Olfactory Mediated Flight Control in Drosophila. *J. Vis. Exp.* **33**, 41–6.

Egelhaaf, M. (1985). On the neuronal basis of figure-ground discrimination by relative motion in the visual system of the fly. *Biol. Cybern.* **52**, 195–209.

Fenk, L. M., Poehlmann, A. and Straw, A. D. (2014). Asymmetric processing of visual motion for simultaneous object and background responses. *Curr. Biol.* **24**, 2913–9.

Ferris, B. D., Green, J. and Maimon, G. (2018). Abolishment of Spontaneous Flight Turns in Visually Responsive Drosophila. *Curr. Biol.* **28**, 170-180.e5.

Fox, J. L., Aptekar, J. W., Zolotova, N. M., Shoemaker, P. A. and Frye, M. A. (2014). Figure-ground discrimination behavior in Drosophila. I. Spatial organization of wing-steering responses. *J. Exp. Biol.* **217**, 558–69.

Gonzalez-Bellido, P. T., Wardill, T. J. and Juusola, M. (2011). Compound eyes and retinal information processing in miniature dipteran species match their specific ecological demands. *Proc. Natl. Acad. Sci.* **108**, 4224–4229.

Gotz, K. G. (1965). Die optischen Übertragungseigenschaften der Komplexaugen von Drosophila. *Kybernetik* **2**, 215–221.

Hateren and Schilstra (1999). Blowfly flight and optic flow. II. Head movements during flight. *J. Exp. Biol.* **202 (Pt 11**, 1491–500.

Heisenberg, M. and Buchner, E. (1977). The role of retinula cell types in visual behavior of Drosophila melanogaster. *J. Comp. Physiol. A* **117**, 127–162.

Juusola, M., Dau, A., Song, Z., Solanki, N., Rien, D., Jaciuch, D., Dongre, S., Blanchard, F., de Polavieja, G. G., Hardie, R. C., et al. (2016). Microsaccadic information sampling provides Drosophila hyperacute vision. *Elife* **6**, e26117.

Juusola, M., Dau, A., Song, Z., Solanki, N., Rien, D., Jaciuch, D., Dongre, S. A., Blanchard, F., de Polavieja, G. G., Hardie, R. C., et al. (2017). Microsaccadic sampling of moving image information provides Drosophila hyperacute vision. *Elife* **6**,.

Keleş, M. F., Mongeau, J.-M. and Frye, M. A. (2019). Object features and T4/T5 motion detectors modulate the dynamics of bar tracking by Drosophila. *J. Exp. Biol.* **222**, jeb190017.

Kitaoka A (2002). Trick Eyes. *Tokyo: Kanzen*.

Kunze, P. (1961). Untersuchung des Bewegungssehens fixiert fliegender Bienen. *Z. Vgl. Physiol.* **44**, 656–684.

Land, M. F. (1997). Visual Acuity in Insects. *Annu. Rev. Entomol.* **42**, 147–177.

Land, M. F. and Nilsson, D.-E. (2012). *Animal Eyes*. 2nd ed. Oxford University Press.

MacWilliams, F. J. and Sloane, N. J. A. (1976). Pseudo-random sequences and arrays. *Proc. IEEE* **64**, 1715–1729.

Martinez-Conde, S. and Macknik, S. L. (2017). Unchanging visions: the effects and

limitations of ocular stillness. *Philos. Trans. R. Soc. Lond. B. Biol. Sci.* **372**,.

Mongeau, J.-M. and Frye, M. A. (2017). Drosophila Spatiotemporally Integrates Visual Signals to Control Saccades. *Curr. Biol.* **27**, 2901-2914.e2.

Mongeau, J.-M., Cheng, K. Y., Aptekar, J. and Frye, M. A. (2019). Visuomotor strategies for object approach and aversion in Drosophila melanogaster. *J. Exp. Biol.* **222**,.

O'Carroll, D. C. and Wiederman, S. D. (2014). Contrast sensitivity and the detection of moving patterns and features. *Philos. Trans. R. Soc. B Biol. Sci.* **369**, 20130043.

Otero-Millan, J., Macknik, S. L. and Martinez-Conde, S. (2012). Microsaccades and blinks trigger illusory rotation in the "rotating snakes" illusion. *J. Neurosci.* **32**, 6043–51.

Reichardt, W. and Poggio, T. (1979). Figure-ground discrimination by relative movement in the visual system of the fly. *Biol. Cybern.* **35**, 81–100.

Reiser, M. B. and Dickinson, M. H. (2008). A modular display system for insect behavioral neuroscience. *J. Neurosci. Methods* **167**, 127–39.

Sherman, A. and Dickinson, M. H. (2003). A comparison of visual and haltere-mediated equilibrium reflexes in the fruit fly Drosophila melanogaster. *J. Exp. Biol.* **206**, 295–302.

Snyder, A. W. (1979). Physics of Vision in Compound Eyes. In *Comparative Physiology and Evolution of Vision in Invertebrates: A: Invertebrate Photoreceptors* (ed. Autrum, H.), pp. 225–313. Berlin, Heidelberg: Springer Berlin Heidelberg.

Srinivasan, M. V. (1993). Even insects experience visual illusions. *Curr. Sci.* **64**, 649–655.

Tammero, L. F., Frye, M. A. and Dickinson, M. H. (2004). Spatial organization of visuomotor reflexes in Drosophila. *J. Exp. Biol.* **207**, 113–122.

Troncoso, X. G., Macknik, S. L., Otero-Millan, J. and Martinez-Conde, S. (2008). Microsaccades drive illusory motion in the Enigma illusion. *Proc. Natl. Acad. Sci. U. S. A.* **105**, 16033–8.

Tuthill, J. C., Chiappe, M. E. and Reiser, M. B. (2011). Neural correlates of illusory motion perception in Drosophila. *Proc. Natl. Acad. Sci. U. S. A.* **108**, 9685–90.

FIGURE LEGENDS

Figure 1. Magnetic tether paradigm and control framework. A) Flies are suspended within a magnetic field and free to rotation about the yaw axis. LED panels wrap 360° around the fly. A high-speed camera records the fly's bottom position. B) Closed-loop control diagram of flight in the magnetic tether. With a static panorama, flies generate body motion that generates visual reafference. The difference between motion and reafference generates some error (retinal slip). C) Left: Diagram of compound eye ommatidia mosaic. The separation distance between each ommatidium define the inter-ommaditial angle $\Delta\varphi$. The distance about the horizontal axis is considered for vertical gratings. Right: Grating defined by spatial wavelength λ. D) Contrast ratio (actual divided by perceived contrast) as a function of spatial wavelength for *Drosophila melanogaster*. Acceptance angle $\Delta\rho = 5°$ for the simulation. At $\lambda = 7.5°$, the contrast ratio is ~1%. E) Closed-loop control diagram. Inset: Proposed parallel visual motion processing pathway for object tracking and background stabilization.

Figure 2. Gratings of spatial wavelength below Nyquist wavelength destabilizes the gaze stabilization reflex. A) Top panels: Example 25 s trials for the same fly presented a static 7.5° (left) and 15° (right) spatial wavelength pattern. Bottom panels: Angular speed data. The grey dotted line is the calculated threshold for saccade detection. The inset shows the drift generated by the 7.5° static background. Arrows indicate inter-saccade intervals, with marked differences between 7.5° (yaw drift) and 15° (no yaw drift) spatial wavelengths. B) Simulation of two-dimensional flight trajectory fly heading data by prescribing a fixed flight speed (30 cm s^{-1}). For visual clarify, a randomly selected subset of trials is showed (grey lines) and three trials are highlighted in red. C) Angular heading data (with saccades removed) for six static gratings of different spatial wavelength and a randomly textured grating. Trials for flies that drifted

predominantly in the CW (left panel) and CCW direction (right panel). D) Box plot of net heading angles for data in C. E) Speed of flies for data showed in C,D. F) Drift speed in magnetic tether with a paper drum of λ = 7.5° and 9°. 7.5°: n = 15 flies, 75 trials; 9°: n = 12 flies, 60 trials. G) Drift speed in magnetic tether with higher spatial resolution (each pixel subtending 1.9°). n = 5 flies, 25 trials. The drift speed is statistically significant between 3.75° and 7.5° (p<0.001). H) Spontaneous saccade dynamics. For C−E and H, n = 36 flies.

Figure 3. Perceptual aliasing in closed loop. A) Proposed interpretation of perceptual aliasing in closed loop. A mismatch between the sign of the perceived motion direction (V_p) and the actual body velocity (V_f) elicits a non-zero body velocity due to a non-zero error e, corresponding to the observed drift in the magno tether. B) Hassenstein-Reichardt EMD model with spatial filter (S), first-order, low-pass filter (LP), multiplication nonlinearity (×), summation (Σ) and inter-ommatidial distance ($\Delta\varphi$). C) EMD steady-state response of analytical model as a function of spatial frequency for a fixed temporal frequency of 2 Hz. Shaded region: aliasing of visual input. D) EMD steady-state response of analytical model for distinct spatial wavelengths λ. For visual clarity, the 3.75° and 15° EMD responses were offset as they fully overlap. E) Same a D) but for a computational EMD model with a discrete low-pass filter and spatial filter simulating *Drosophila* optics. For all simulations, we used $\Delta\varphi$ = 4.5°.

Figure 4. Gaze fixation is not necessary for object detection and pursuit. A) Sample 25 s trials for a bar moving over a randomly textured background moving counter-directionally (top) and bar moving over a λ = 7.5° static background for the same fly (bottom). Top: Flies generate bouts of smooth pursuit gaze stabilization (black arrowhead) interspersed with object tracking saccades (green arrowhead). As a wide-field stimulus, the background absolute angle is arbitrary but is shown here for reference. Bottom: Flies drifted in the presence of a static background and

generated tracking between bouts of drifting. B) Left: Tracking saccade count for a textured bar moving anti-directionally to a randomly textured ground. Right: Tracking saccade count for a textured bar moving on a λ = 7.5° ground. n = 32 flies, 18,189 saccades total; 3,195 tracking saccades total.

Figure 5. Rigid tether paradigm indicates that aliasing effects are induced by body motion. A) A fly is suspended within a virtual reality arena and wing motion is tracked to infer steering effort via changes in wing-beat amplitude (ΔWBA). B) Open-loop control diagram of rigid tether paradigm. C) Wing steering responses (ΔWBA) to static random (left) and λ = 7.5° grating (right). Thick black line: mean: Gray area: ± 1 STD. Colored lines represent the mean for each individual fly. D) Top: pseudo-random sequence of object position. Bottom: Wing steering response from one fly to sequence. E) Example impulse response function between visual stimulus and steering for one fly tested at one azimuthal location. The unit of response amplitude on the scale bar is uncalibrated ΔWBA (V deg sec or Volt degree second). F) Impulse responses to pseudo-random object motion are measured at 24 azimuthal locations and assembled into a Spatio-Temporal Action Field (STAF) for n = 12 flies.

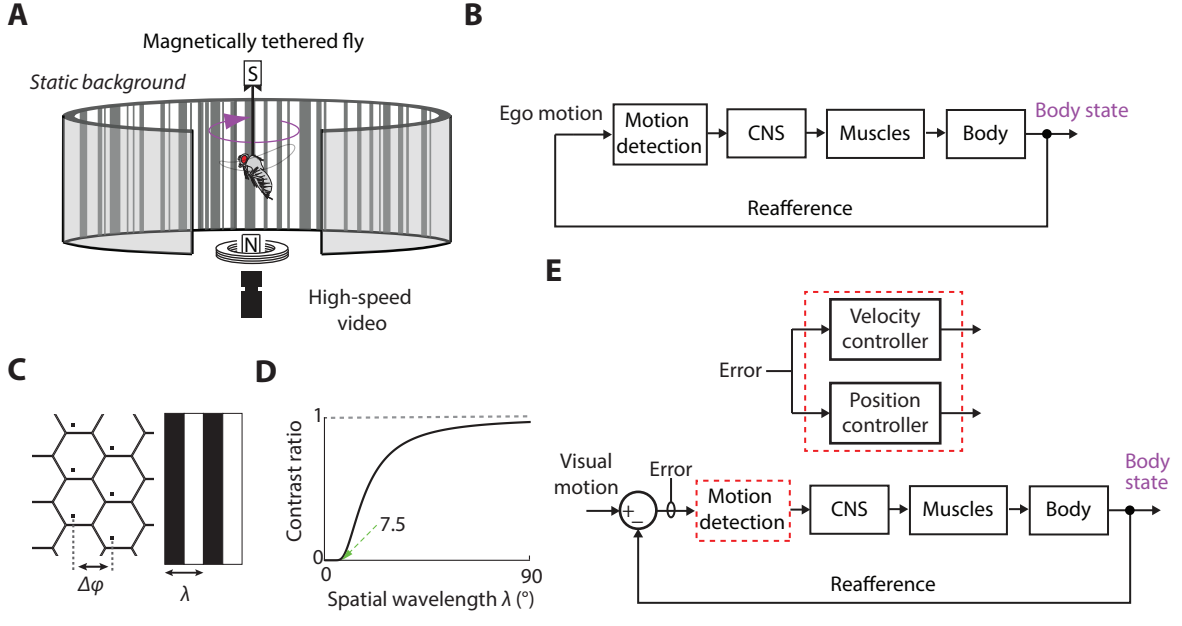
A
Magnetically tethered fly
Static background
S
N
High-speed
video
B
Ego motion
Motion
detection
CNS
Muscles
Body
Body state
Reafference
C
Δφ
λ
D
Contrast ratio
1
0
7.5
0
90
Spatial wavelength λ (°)
E
Error
Velocity
controller
Position
controller
Visual
motion
Error
Motion
detection
CNS
Muscles
Body
Body
state
Reafference

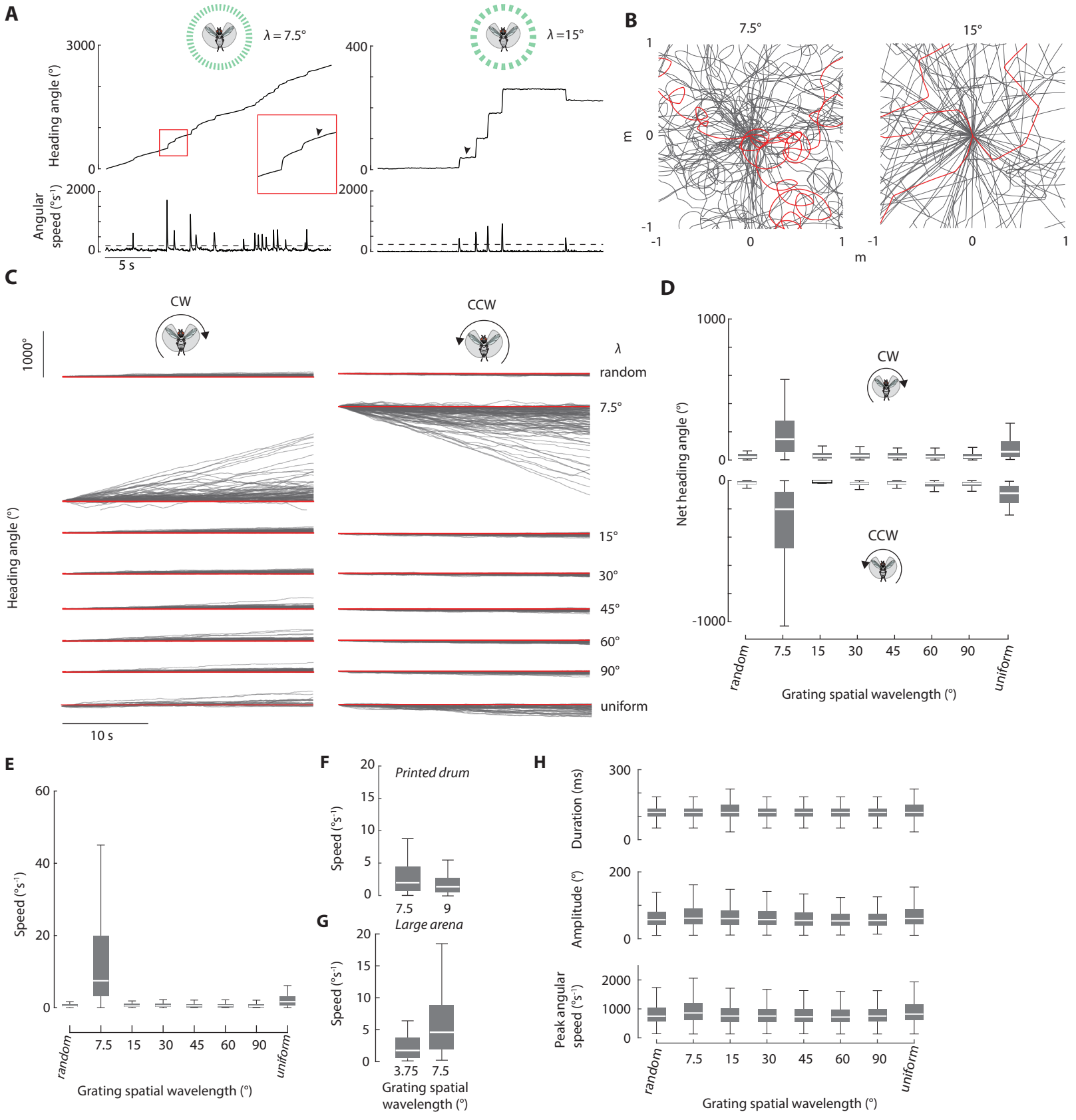
A
λ = 7.5°
λ =15°
Heading angle (°)
Angular speed (°s⁻¹)
5 s
B
7.5°
15°
m
C
CW
CCW
1000°
λ
random
7.5°
15°
30°
45°
60°
90°
uniform
Heading angle (°)
10 s
D
CW
CCW
Net heading angle (°)
random
7.5
15
30
45
60
90
uniform
Grating spatial wavelength (°)
E
Speed (°s⁻¹)
Grating spatial wavelength (°)
F
Printed drum
Speed (°s⁻¹)
G
Large arena
Grating spatial wavelength (°)
H
Duration (ms)
Amplitude (°)
Peak angular speed (°s⁻¹)
Grating spatial wavelength (°)

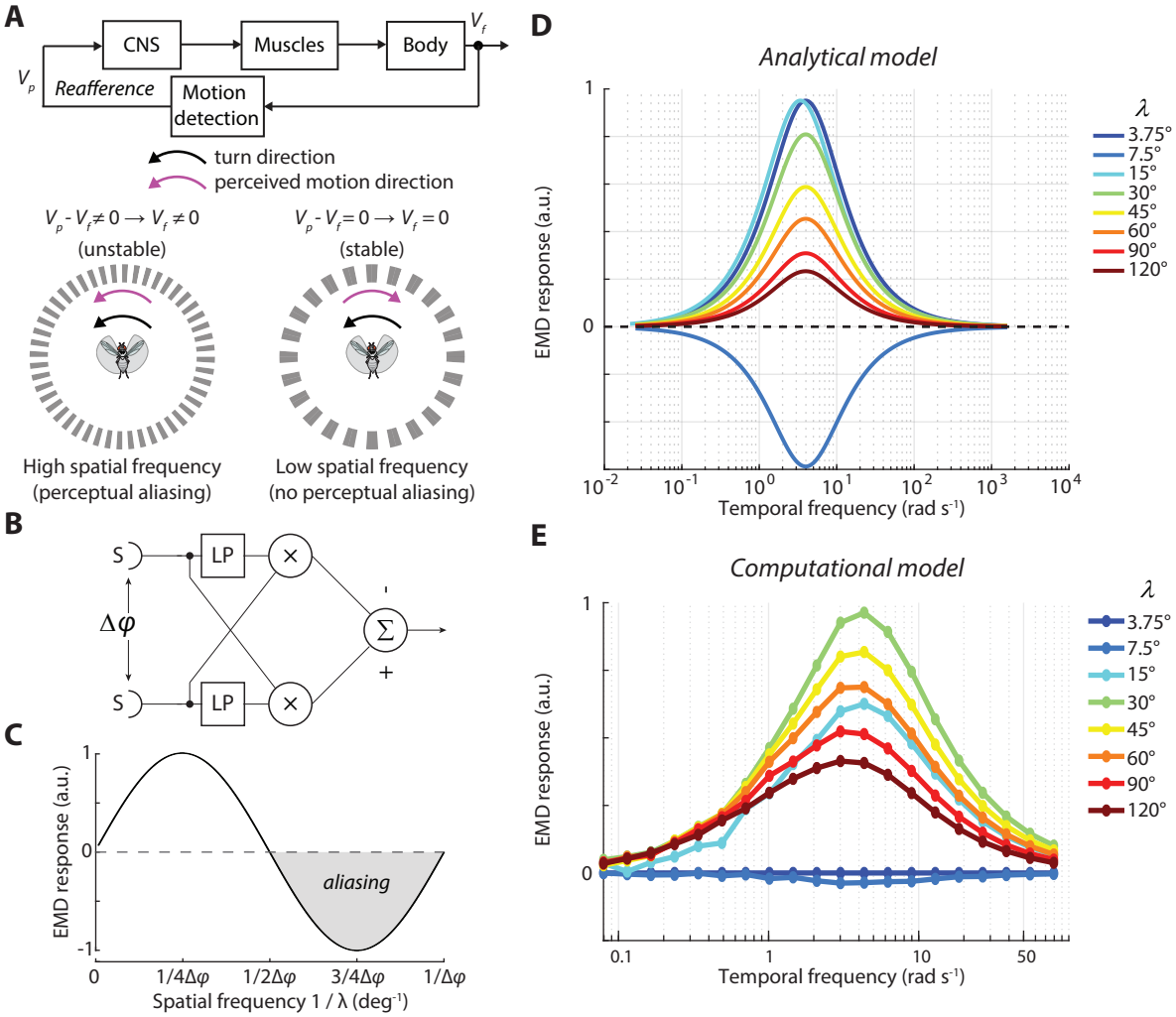
A
CNS
Muscles
Body
V_f
V_p
Reafference
Motion detection
turn direction
perceived motion direction
$V_p - V_f \neq 0 \rightarrow V_f \neq 0$
(unstable)
$V_p - V_f = 0 \rightarrow V_f = 0$
(stable)
High spatial frequency
(perceptual aliasing)
Low spatial frequency
(no perceptual aliasing)
B
S
LP
×
Δφ
Σ
+
-
C
EMD response (a.u.)
aliasing
0
1/4Δφ
1/2Δφ
3/4Δφ
1/Δφ
Spatial frequency 1 / λ (deg⁻¹)
D
Analytical model
EMD response (a.u.)
Temporal frequency (rad s⁻¹)
λ
3.75°
7.5°
15°
30°
45°
60°
90°
120°
E
Computational model
EMD response (a.u.)
Temporal frequency (rad s⁻¹)

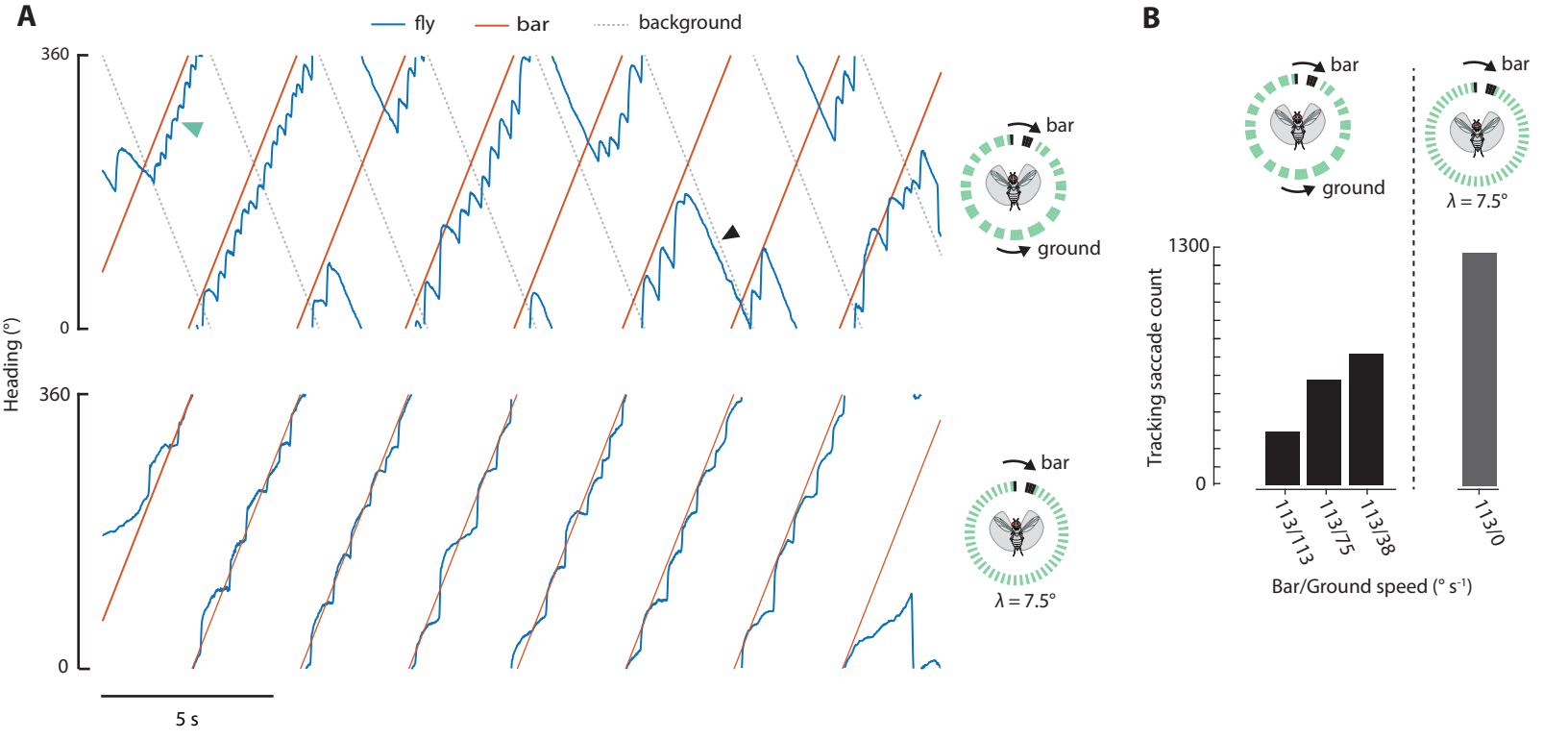
A
fly
bar
background
360
0
Heading (°)
bar
ground
360
0
bar
λ = 7.5°
5 s
B
bar
ground
bar
λ = 7.5°
1300
0
Tracking saccade count
113/113
113/75
113/38
113/0
Bar/Ground speed (° s-1)

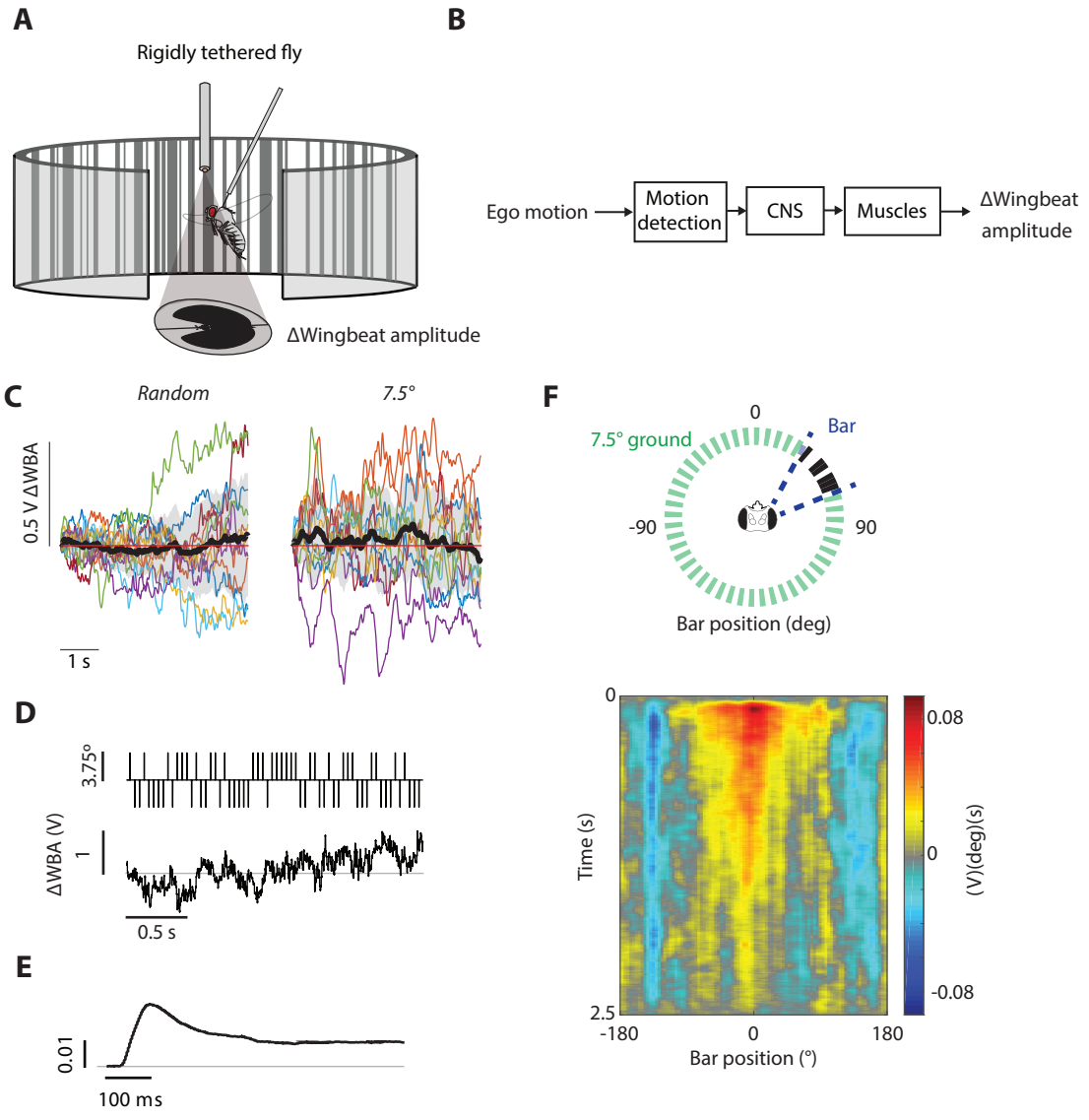
A
Rigidly tethered fly
ΔWingbeat amplitude
B
Ego motion
Motion detection
CNS
Muscles
ΔWingbeat amplitude
C
Random
7.5°
0.5 V ΔWBA
1 s
D
3.75°
ΔWBA (V)
1
0.5 s
E
0.01
100 ms
F
0
7.5° ground
Bar
-90
90
Bar position (deg)
0
Time (s)
2.5
-180
0
180
Bar position (°)
0.08
0
-0.08
(V)(deg)(s)